Biology of Reproduction, 2021, 105(5), 1205–1220
https://doi.org/10.1093/biolre/ioab148
Research Article
Advance Access Publication Date: 2 August 2021

Research Article

Deletion of Gremlin-2 alters estrous cyclicity and disrupts female fertility in mice†

Robert T. Rydze[1,2,‡], Bethany K. Patton[3,4,‡], Shawn M. Briley[3,5], Hannia Salazar Torralba[3], Gregory Gipson[6], Rebecca James[3], Aleksandar Rajkovic[7,8,9], Thomas Thompson[6] and Stephanie A. Pangas[3,4,5,10,*]

[1]Division of Reproductive Endocrinology and Infertility, Department of Obstetrics and Gynecology, Baylor College of Medicine and Texas Children's Hospital Pavilion for Women, Houston, TX, USA, [2]Graduate Program in Clinical Scientist Training, Baylor College of Medicine, Houston, TX, USA, [3]Department of Pathology and Immunology, Baylor College of Medicine, Houston, TX, USA, [4]Graduate Program in Molecular and Cellular Biology, Baylor College of Medicine, Houston, TX, USA, [5]Graduate Program in Biochemistry and Molecular Biology, Baylor College of Medicine, Houston, TX, USA, [6]Department of Molecular Genetics, Biochemistry, and Microbiology, University of Cincinnati College of Medicine, Cincinnati, OH, USA, [7]Department of Pathology, University of California, San Francisco, CA, USA, [8]Department of OB-GYN, University of California, San Francisco, CA, USA, [9]Institute of Human Genetics, University of California, San Francisco, CA, USA and [10]Department of Molecular and Cellular Biology, Baylor College of Medicine, Houston, TX, USA

*__Correspondence__: One Baylor Plaza, Baylor College of Medicine, Houston, TX 77030, USA. Tel: +1 713.798.5898; E-mail: spangas@bcm.edu

†__Grant Support__: This work was supported by National Institutes of Health (NIH) grants R01 HD085994 and T32 HD098068 (to S.A.P.), R35 GM134923 (to T.T.), R01 HD070647 and R21 HD074278 (to A.R.), and P30 CA125123 (to Baylor College of Medicine Advanced Technology Cores/Dan L. Duncan Cancer Center). Hormone assays at the UVA Reproductive Research Ligand Assay Core are supported by NIH R24 HD102061.
‡These authors have contributed equally to this work.

Received 16 March 2021; Revised 28 June 2021; Accepted 27 July 2021

Abstract

Members of the differential screening-selected gene aberrative in neuroblastoma (DAN) protein family are developmentally conserved extracellular binding proteins that antagonize bone morphogenetic protein (BMP) signaling. This protein family includes the Gremlin proteins, GREM1 and GREM2, which have key functions during embryogenesis and adult physiology. While BMPs play essential roles in ovarian follicle development, the role of the DAN family in female reproductive physiology is less understood. We generated mice null for *Grem2* to determine its role in female reproduction in addition to screening patients with primary ovarian insufficiency (POI) for variants in *GREM2*. *Grem2*$^{-/-}$ mice are viable, but female *Grem2*$^{-/-}$ mice have diminished fecundity and irregular estrous cycles. This is accompanied by significantly reduced production of ovarian anti-Müllerian hormone (AMH) from small growing follicles, leading to a significant decrease in serum AMH. Surprisingly, as AMH is a well-established marker of the ovarian reserve, morphometric analysis of ovarian follicles showed maintenance of primordial follicles in *Grem2*$^{-/-}$ mice like wild-type (WT) littermates. While *Grem2* mRNA transcripts were not detected in the pituitary, *Grem2* is expressed in hypothalami of WT female mice, suggesting the potential for dysfunction in multiple tissues composing the hypothalamic–pituitary-ovarian axis that contribute to the subfertility phenotype. Additionally, screening 106 women with POI identified one individual with a

heterozygous variant in GREM2 that lies within the predicted BMP-GREM2 interface. In total, these data suggest that *Grem2* is necessary for female fecundity by playing a novel role in regulating the HPO axis and contributing to female reproductive disease.

Summary sentence

Female mice homozygous null for the BMP antagonist, *Grem2*, shows a complex reproductive phenotype, but which appears to primarily result from disruptions in the hypothalamic–pituitary-ovarian axis leading to irregular estrous cycles.

Graphical Abstract

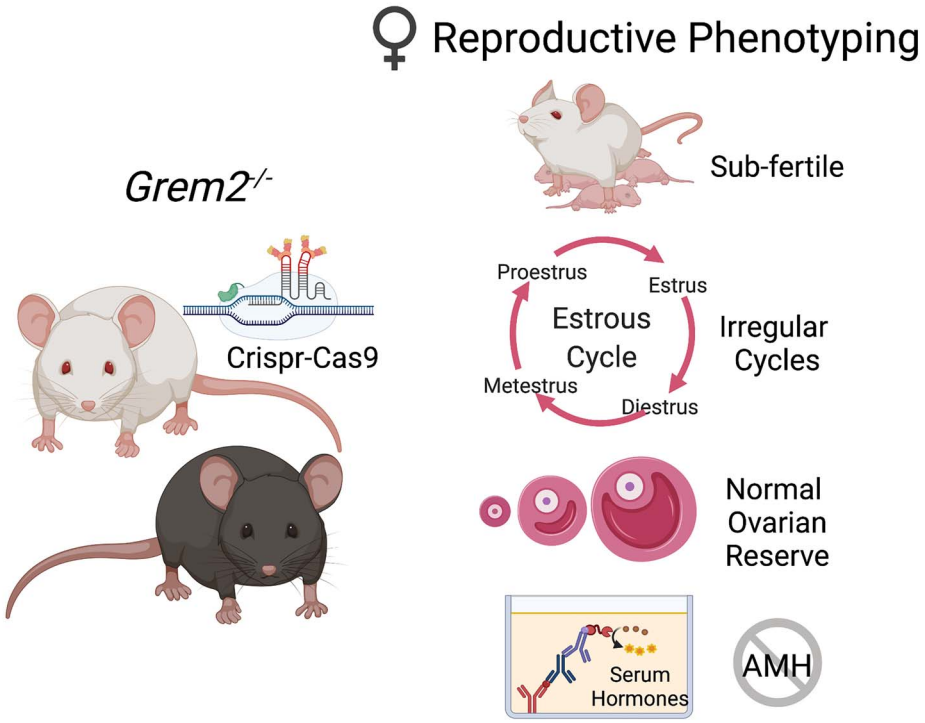

Key words: Gremlin, ovary, folliculogenesis, infertility, reproduction.

Introduction

Gremlin-2 (GREM2) is a member of the "differential screening-selected gene aberration in neuroblastoma" (DAN) family of bone morphogenetic protein (BMP) antagonists and is also known as "protein related to DAN and Cerberus" (PRDC) [1]. *Grem2* was identified in a gene trap for developmentally important genes [2]. The DAN family includes GREM2/PRDC, Gremlin-1 (GREM1), Sclerostin, DAN, Cerberus, Caronte, Coco, and Dante [3]. This protein family is best characterized as extracellular binding proteins that sequester BMPs, thereby preventing them from binding and activating their signaling receptors. GREM2 strongly inhibits BMP signaling [4], but also binds other TGFβ family members, including anti-Müllerian hormone (AMH) and GDF5 [4, 5].

Human genome-wide association studies identified *GREM2* variants associated with developmental disorders and disease, such as osteoporosis, atrial fibrillation, and tooth agenesis [6–9]. A *Grem2*$^{-/-}$ mouse model was previously developed as part of a high-throughput mouse knockout (KO) and phenotyping project, with tooth defects identified as the major phenotype [10]. No fertility defects were reported in male or female *Grem2*$^{-/-}$ mice, although the reproductive phenotyping screen was limited (P. Vogel, personnel communication). A variant of the related *GREM1* has been reported in a patient with primary ovarian insufficiency (POI), but none reported for *GREM2* [11].

There are limited studies characterizing GREM2 function in female reproduction. *GREM2* is expressed in the developing human ovary at 8–21 weeks of gestation, with increasing expression toward the time of primordial follicle formation [12]. Embryonic *Grem2* expression in the developing mouse gonad (male or female) has not been characterized, but *Grem2* is expressed in the mouse and rat ovary in granulosa cells during postnatal follicle development [1]. In vitro studies indicate that GREM2 inhibits BMP4 and AMH, both of which regulate growth dynamics of the primordial to primary follicle transition, but in opposite directions (i.e., BMP4 promotes while AMH inhibits the transition) [1, 5, 13].

Given the above studies implicating GREM2 in ovarian folliculogenesis, we generated a new KO mouse model of *Grem2* to determine its role in mammalian reproduction. In this study, we characterize the initial reproductive phenotype. We found that *Grem2*$^{-/-}$ females are subfertile with a primary defect in reproductive cyclicity and significant reductions in ovarian and serum AMH. Despite reduced levels of AMH, the primordial follicle pool was maintained in adult

females. Using POI patient samples, we additionally identified a novel nonsynonymous mutation in *GREM2*. These data suggest that GREM2 may be required to regulate reproductive function in both mice and humans, possibly at multiple levels within the HPO axis.

Materials and methods

Generation of *Grem2* $^{-/-}$ mice

All studies using experimental animals or human subjects were conducted in accordance with the relevant institutional and national guidelines and standards. Experimental animals were used in accordance with the National Institutes of Health Guide for the Care and Use of Laboratory Animals, and this study was approved by the Institutional Animal Care and Use Committee at Baylor College of Medicine (BCM, animal protocol AN-4762). A *Grem2* null allele was generated at the Embryonic Stem Cell and Genetically Engineered Mouse Cores at BCM. Single guide RNA (sgRNA) sequences flanking exon 2 (upstream sgRNA 5'-GGGGTAGATGGTGCTACTTC *CGG*; downstream sgRNA, 5'-GAAAAATCTTGTCGAGTTTC *TGG*; protospacer adjacent motif (PAM) sequences are in italics) were selected with the CRISPR Design Tool [14]. DNA templates for in vitro transcription of sgRNAs were produced using overlapping oligonucleotides in a high-fidelity PCR reaction [15]. sgRNA was transcribed using the MEGA Shortscript T7 kit (ThermoFisher, Waltham, MA). Cas9 mRNA was purchased from ThermoFisher. Cas9 mRNA (100 ng/μL) and sgRNA (10 ng/μL) were microinjected into the cytoplasm of 100 pronuclear stage C57Bl/6 J embryos then transferred to recipient females.

Potential founders were genotyped using the following primers: (P1: 5'-TGTTGTTGTTGTTGACAAAATACTTG; P2: 5'-AATACG-AGAAAGCCGTGCTG; P3: 5'-AAAGAGGTGGTGGTGTCCAG) to identify the wild-type (WT) allele (251 bp) and deletion allele (510–520 bp). Founders were validated by sequencing. Two founder mice were selected for initial characterization. Founder mice were backcrossed to *C57BL/6; 129S7/SvEvBrd* F1 hybrid mice to reduce the potential off-target mutation effects prior to homozygous matings to generate the experimental *Grem2*$^{-/-}$. WT mice of the same genetic background were used as controls.

Fertility studies

Breeding pairs were established between sexually mature (6–8 weeks old) WT or KO female mice with 8-week-old WT males (F1 *C57BL/6; 129S7/SvEvBrd*) and continuously housed for 8 months. Number and date of pups born at 4-week intervals (one "month") were recorded. For estrous cycle analysis, 6-month WT and KO mice were individually housed with enrichment (EnviroPak, Lab Supplies, Dallas, TX). Vaginal lavage and cytology was performed daily for 1 month as described [16].

Histologic analysis

Mice were weighed, anesthetized by isoflurane (Abbott Laboratories, Abbott Park, IL), and euthanized by cervical dislocation. Estrous stage was verified at time of necropsy. Ovaries were fixed in 10% neutral buffered formalin (Electron Microscopy Sciences, Hatfield, PA) and processed and embedded at the BCM Human Tissue Acquisition and Pathology Core. Manual follicle counts were performed as described [17]; 3-week-old ovaries were serially sectioned at 5 μm and all sections retained. Slides were stained in periodic acid-Schiff (Sigma, St. Louis, MO). Follicles containing an oocyte with a visible nucleus were counted in every fifth section to avoid double counting oocytes. Final values of preantral follicles were multiplied by a correction factor of 5 based on published methodologies [18].

Hormone analysis

Blood was retrieved from isoflurane-anesthetized diestrus mice by cardiac puncture. Serum was separated in microtainer collection tubes (SST BD Microtainer, Becton, Dickinson and Company, Franklin Lakes, NJ) and stored at −20 °C. Hormones were quantified at the University of Virginia Ligand and Assay Core: estradiol (ELISA, CalBiotech, Spring Valley, CA USA), follicle stimulating hormone (FSH)/luteinizing hormone (LH) (ELISA, EMD Millipore, Saint Charles, MO USA), AMH (ELISA, Ansh Laboratory, Webster, TX USA), and testosterone (ELISA, IBL, Minneapolis, MN USA). Assay method information is available online at https://med.virginia.edu/research-in-reproduction/ligand-assay-analysis-core/assay-methods/. For statistical analysis, values that fell below the threshold of detection were set to the value of the lower limit of detection [19] as previously described [20] ELISA data were log transformed prior to statistical analysis.

Superovulation experiments

Female mice (5 weeks of age) were given i.p. injections of 5 IU equine chorionic gonadotropin for 46 h, followed by 5 IU human chorionic gonadotropin. Mice were euthanized the following morning, and oocytes were collected from the oviduct into minimal essential medium with 0.3-mg/mL hyaluronidase (Sigma, St. Louis, MO) and counted following removal of the cumulus cells. Experiments were performed on littermates from three independent litters and on different days.

Immunohistochemistry and immunofluorescence

Immunohistochemistry was performed as described [21] for the macrophage marker F4/80 (catalog #AB6640, Abcam, Cambridge, UK, 1:100). For AMH immunofluorescence, tissue sections were antigen retrieved in 0.01 M citric acid and 0.1% Triton X (Sigma, St. Louis, MO), blocked with the avidin/biotin blocking kit (Vector Laboratories, Burlingame, CA) and 3% BSA in Tris-buffered saline (TBS), then incubated overnight at 4 °C with goat anti-AMH (1:250; catalog #6886, Santa Cruz Biotechnology, Santa Cruz, CA). Slides were washed in TBS-0.1%Tween (TBS-T), incubated at room temperature with Alexa Fluor rabbit anti-goat 594 (Invitrogen, Waltham, MA; 1:250) for 1 h, washed, incubated in 4′6′-diamidino-2-phenylindole (DAPI) (1:1000) in TBS for 5 min, and mounted in anti-fade Vectashield (Vector Laboratories, Burlingame, CA). Fluorescent images were captured using a Nikon A1R-s confocal laser scanning microscope at the BCM Integrated Microscopy Core and processed with the Nikon Perfect Focus System (Nikon Corporation, Japan). Exposure times were held constant between WT and *Grem2*$^{-/-}$ samples. Representative follicles within ovary section were analyzed using ImageJ software (ImageJ 1.52a Wayne Rasband, National Institutes of Health, USA http://imagej.nih.gov/ij) to measure the mean fluorescence intensity. Follicles were classified as described [22].

Quantitative PCR

Ovaries were collected in RNA later (Ambion, Austin, TX), incubated overnight at 4 °C, then stored at −80 °C. RNA was isolated using the RNeasy Micro kit (Qiagen, Valencia, CA) with in column DNase treatment (Qiagen, Valencia, CA) following the manufacturer's protocol. RNA concentration was quantified using a NanoDrop Spectrophotometer ND-1000 (NanoDrop Technologies, Wilmington, DE). Complementary DNA was synthesized from

200 ng of total RNA with the High-Capacity RNA-to-cDNA reverse transcription kit (Life Technologies, Waltham, MA). Real-time quantitative PCR (qPCR) assays were performed on an Applied Biosystems StepOne machine using TaqMan Fast Master mix and predesigned primer-probe mixes for *Grem2* (FAM labeled Mm00501909_m1) and *Gapd* (FAM labeled Mm00484668_m1) or Fast SYBR Green Master Mix (Life Technologies, Waltham, MA) with custom primers chosen from validated qPCR primer sets at Primer Bank (https://pga.mgh.harvard.edu/primerbank/). Primer sequences are available upon request. Melt curve analysis was used to validate a single amplification peak when using SYBR Green Master Mix. Relative level of transcript was calculated using the ΔΔCT method [23] with the housekeeping gene *Gapd* used for normalization and data shown mean to the relative level in WT ovaries.

POI patient sample analysis and protein modeling

Whole exome sequence (WES) data were analyzed from two published datasets [24, 25]. These data included 103 patients diagnosed with POI at the University of Pittsburgh under the approved Institutional Review Board protocols (PRO09080427). Informed consent was obtained from all individual participants. Gene variants were evaluated using the guidelines of the American College of Medical Genetics and Genomics, which recognizes five classes of variants: benign, likely benign, uncertain significance, likely pathogenic, and pathogenic [26]. Variants with minor allelic frequency in the Exome Aggregation Consortium (ExAC) database >1% were excluded. Variants not present in the 1000 Genomes Project, Exome Variant Server data sets, Exome Aggregation Consortium (ExAC, Cambridge, MA), or the Single Nucleotide Polymorphism database (dbSNP) were considered novel variants [27–29]. Protein modeling was performed as described [4] using PyMol (The PyMol Molecular Graphics System, Schrödinger, LLC, New York, NY).

Statistical analyses

GraphPad Prism 5 (GraphPad Software, La Jolla, CA) was used for statistical analysis. Two-tailed unpaired Student *t*-test or the nonparametric Mann–Whitney U was used for single comparisons. One-way analysis of variance followed by Fisher least significant difference test or Bonferroni's Multiple Comparison test was used for multiple comparisons. Data that are not normally distributed (e.g., hormone data and qPCR data) were log transformed prior to statistical analysis. Linear regression was used to assess correlation between FSH and estradiol levels. A power analysis was performed for all experimental methods, and sample sizes are indicated in the text and figure legends; a minimum of three independent experiments was always carried out, with $P < 0.05$ considered statistically significant.

Results

Generation and validation of a *Grem2* $^{-/-}$ mouse model

A null allele for *Grem2* was engineered using CRISPR/Cas9 genome editing (Figure 1). Two sgRNAs were designed to target Cas9 to flanking regions of exon 2, generating an approximately one kilobase deletion that contains the splice acceptor site in exon 2, the entire coding region, and portions of the 3' untranslated region (UTR; Figure 1A). Exon 1, which encodes the 5′ UTR, and elements of the 3' UTR remain. sgRNA was injected into pro-nuclear stage embryos along with *Cas9* mRNA. Nonhomologous end joining (NHEJ)-mediated repair of the two double stranded breaks (DSBs) created by sgRNA targeted Cas9 should result in a null allele through loss of exon 2. Seventeen live-born mice were obtained from 100 injected and transferred embryos. PCR genotyping indicated that 4 pups contained a molecular weight band that approximated the predicated size of the deletion (Figure 1B). Different deletion sizes are produced in each founder because of the imprecise nature of NHEJ and DSB repair. DNA from the four potential founders was sequenced, and two potential founder alleles aligned with the expected deletion (Figure 1C). These mice were individually crossed to F1 mixed hybrid strain *C57BL/6/129S7/SvEvBrd*, the genetic background of our previous studies on BMP and GREM1 [30, 31]. Breeding to the WT strain ensures germline transmission of the correct allele and reduces the probability of carryover of potential off-target mutations. Homozygous mice for both founder lines were generated from heterozygous crosses and were produced at normal Mendelian ratios for both founders. Male and female homozygous mice were viable. No difference in phenotype was detected in initial studies of offspring between founder lines (e.g., incisor defects and fertility testing), so the founder line that contained the larger deletion ("P2" Figure 1B) was chosen for further characterization.

We confirmed the loss of *Grem2* expression by measuring mRNA levels by qPCR in tissues known to highly express the transcript (i.e., ovary and lung). *Grem2* transcript levels were undetectable in either tissue in *Grem2*$^{-/-}$ mice (Figure 1D). As a previous *Grem2*$^{-/-}$ model showed incisors defects [10], we also measured incisor length. Like the previous model, sexually mature (i.e., over 6 weeks of age) *Grem2*$^{-/-}$ female mice had defects in incisor length that mainly affected the upper incisors (Figure 1E). This did not impact body weight, as *Grem2*$^{-/-}$ females had similar body weights to WT mice at 3 weeks of age, were slightly but significantly larger at 6 and 12 weeks, but had similar body weight to WT mice at 24 weeks of age, all of which fell within the range considered normal for adult C57/BL6 and 129SvEv mouse lines (Figure 2A) [32].

Loss of *Grem2* reduced female fecundity

To test the effect of *Grem2* loss on female fertility, 6–8 weeks old WT and *Grem2*$^{-/-}$ female mice were pair bred with sexually mature (8-week-old) WT males continuously for 8 months and the number of pups per litter and litters per month were recorded. Overall, WT females gave birth to an average of 9.2 ± 0.3 pups per litter and 1.1 ± 0.02 L per month (Figure 2B and C). *Grem2*$^{-/-}$ females gave birth to similar numbers of pups per litter (8.9 ± 0.5) (Figure 2B). However, if age is considered, a small but statistically significant decline of 22% in pups per litter was detected in older *Grem2*$^{-/-}$ females when breeding data were split into two age groups ($P = 0.03$) (Figure 2B). In addition, there was a significant decrease in the numbers of litters per month in *Grem2*$^{-/-}$ females (0.67 ± 0.05) compared with WT females (1.02 ± 0.02) ($P = 0.001$) (Figure 2C). *Grem2*$^{-/-}$ females showed a decrease in litters per month regardless of age; during months 1–4, *Grem2*$^{-/-}$ female mice missed an average of 1.2 ± 0.2 L (compared with 0 for the WT), and during months 5–8, *Grem2*$^{-/-}$ female mice missed 1.8 ± 0.2 L (compared with 0 for the WT). Thus, loss of *Grem2* caused female subfertility that appears to be primarily driven by a reduction in litters per month.

Grem2 $^{-/-}$ females have abnormal estrous cycles

Because of the significant change in litter production, estrous cycles were evaluated in 6-month-old females ($n = 6$ per genotype). WT mice estrous cycles averaged 4–5 days, while *Grem2*$^{-/-}$ female mice had irregular cycles (Figure 3A). *Grem2*$^{-/-}$ females had a significant

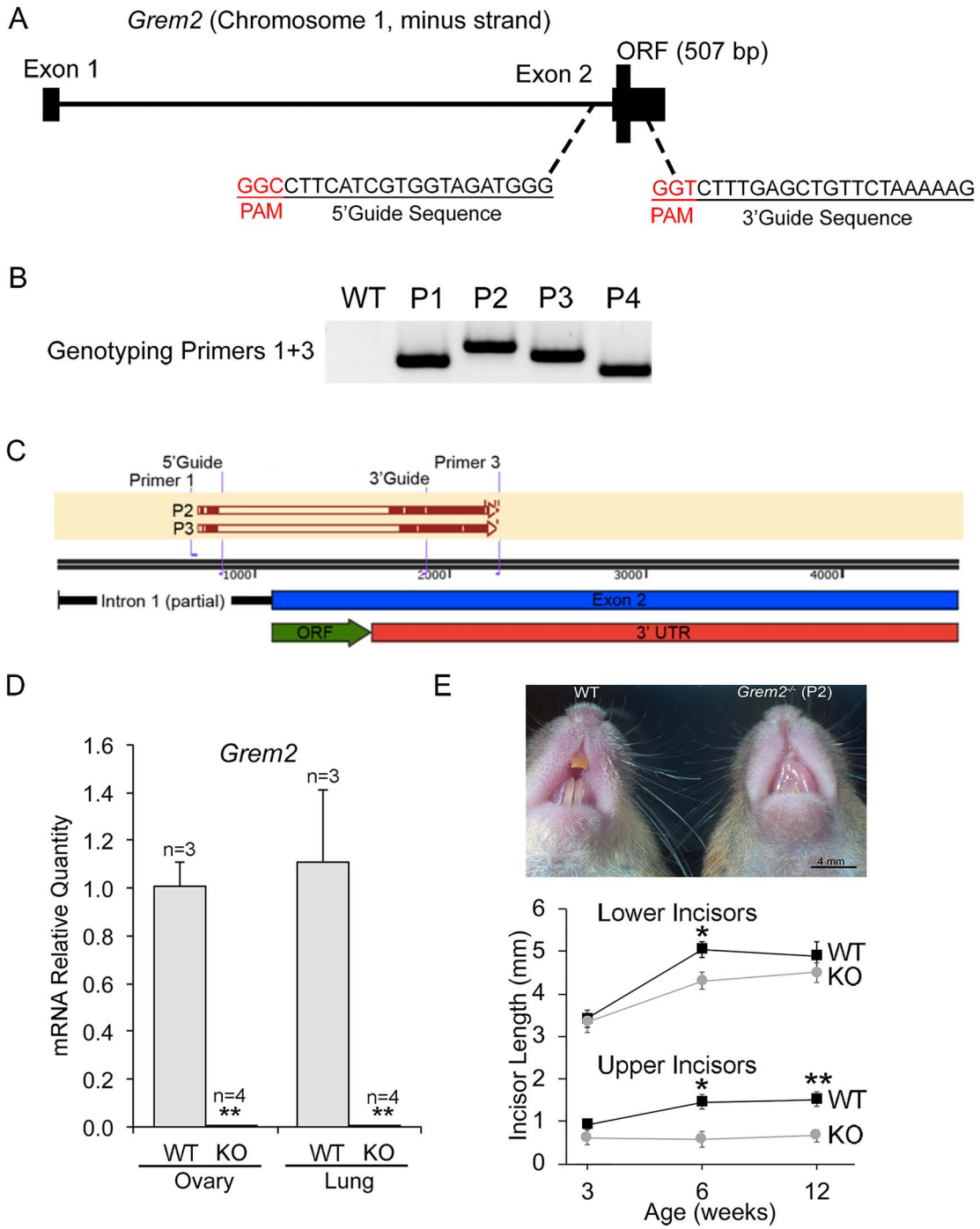

Figure 1. Generation and validation of a *Grem2* null allele. (A) Schematic of the *Grem2* locus on chromosome 1. *Grem2* contains two exons, with the open reading frame (ORF) encoded in exon 2. The 5′ and 3′ guide sequences are shown with the PAM site in red. The 5′ guide sequence is located in intron 1 and the 3′ guide sequence is located within the 3′ UTR. (B) PCR genotyping of genomic DNA of potential founder mice, labeled P1-P4. Different size deletions are typical due to the imprecise nature of NHEJ. (C) Summary of DNA sequencing information and alignment of the founders P2 and P3 with the location of the ORF shown in green and the 3′ UTR in red. (D) Validation of loss of *Grem2* transcript in *Grem2*$^{-/-}$ tissues by qPCR, $n=3$ independent ovaries for WT and $n=4$ for KO, $^{**}P<0.01$. Levels are normalized to *Gapd* and shown relative to the amount in the WT ovary. (E) Comparison of incisors between WT and *Grem2*$^{-/-}$ from the P2 parental line, which was chosen from 2 founder lines with similar fertility defects. Graph shows data for upper and lower incisors in WT and *Grem2*$^{-/-}$ at three ages. No difference was found in upper or lower incisor length between WT and *Grem2*$^{-/-}$ at 3 weeks of age ($n=6$ mice each genotype). Lower and upper incisors of Grem2$^{-/-}$ ($n=5$ mice) were significantly smaller at 6 weeks of age ($^{*}P<0.05$) but only upper incisors were significantly smaller ($^{**}P<0.01$) in *Grem2*$^{-/-}$ ($n=5$) compared with WT ($n=5$) at 12 weeks of age. Image insert, WT, and *Grem2*$^{-/-}$ incisors at 9 months of age. Scale bar in photograph, 4 mm.

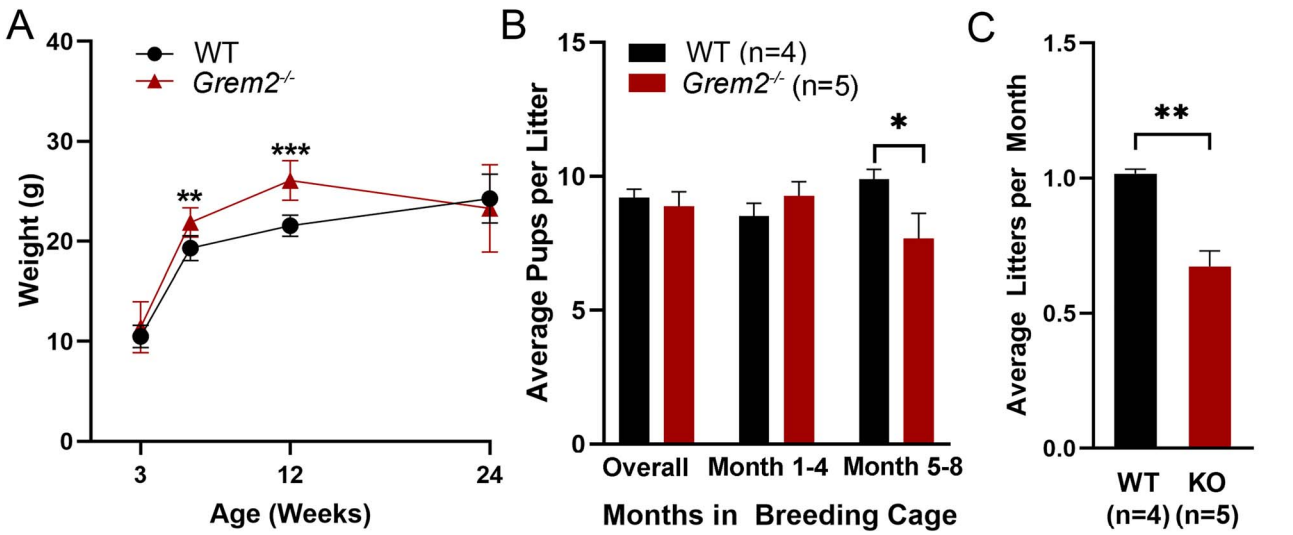

Figure 2. *Grem2*$^{-/-}$ females are subfertile. (A) Body weight (g) at time of necropsy for WT (black circles) and *Grem2*$^{-/-}$ (red triangles) females at 3, 6, 12, and 24 weeks of age. Markers represent the mean ± s.e.m. of $n = 3$–14 animals of each genotype, $^{**}P < 0.01$ and $^{***}P < 0.001$ by Student's *t*-test between WT and KO mice at the indicated time point. (B) Average litter sizes (pups per litter) WT (black bars) ($n = 32$ litters from 4 females) and *Grem2*$^{-/-}$ (red bars) ($n = 25$ litters from 5 females) mice. Females of each genotype were set up in breeding pairs at sexual maturity (6–8 weeks of age) to 8-week-old WT males and the number of pups born recorded over 8 months. The average pups per litter is shown as mean ± s.e.m. for the entire breeding trial ("overall"; months 1–8) or in two equal age brackets (1–4 months versus 5–8 months). The overall data were split into two age brackets to determine if there was any effect of age, with the asterisk indicated statistical significance in the 5–8 month group; $^{*}P < 0.05$ by Student's *t*-test. (C) Average litters per month between WT (black bars) and *Grem2*$^{-/-}$ ("KO") females (red bars) in the same 8-month breeding trial as shown in panel B. Data are shown as mean ± s.e.m., with ⁎⁎indicating $P < 0.01$ by Student's *t*-test.

increase in the percentage of days spent in metestrus and diestrus and a concomitant decrease in the number of estrous cycles per month (Figure 3B and C). To determine if there were changes in steady state levels of key reproductive hormones, we measured serum levels of estradiol, testosterone, LH, and FSH in diestrous stage 6-month-old WT and *Grem2*$^{-/-}$ females (Supplementary Table S1); we did not detect any significant changes. However, we additionally used linear regression to test the well-established correlation between estradiol and FSH levels. While diestrus WT mice exhibit the expected correlation between estradiol and FSH ($r^2 = 0.48$), estradiol and FSH are not correlated in diestrus *Grem2*$^{-/-}$ females ($r^2 = 0.07$) (Figure 3D).

To determine if the disruption in estrous cyclicity and litter production was related to altered ovarian follicle development, we analyzed ovarian histology of WT and *Grem2*$^{-/-}$ females at multiple time points (3 weeks, 6 weeks, 12 weeks, and 6 months of age). Upon necropsy, no difference in gross appearance or size of ovaries was noted between genotypes at any age (data not shown). Morphometric analysis of follicles in ovarian histologic sections from sexually immature 3-week mice showed no significant differences in the number or types of follicles including primordial, primary, secondary, antral, or atretic follicles between genotypes and no obvious histologic defects (Figure 4A–C). Furthermore, at 6 or 12 weeks of age, there were no gross histologic differences in ovaries from *Grem2*$^{-/-}$ females compared with WT mice and all stages of follicles including corpora lutea (CL) were present (data not shown). Treatment of sexually immature (5-week-old) females with exogenous hormones to induce ovulation ("superovulation") resulted in similar numbers of eggs retrieved from oviducts of WT and *Grem2*$^{-/-}$ females (Figure 4D). Thus, while litter production was affected at all ages, no histologic defect was found in ovaries from 3 to 12 weeks of age nor was the response to exogenous hormones altered.

At 6 months of age, both WT and *Grem2*$^{-/-}$ ovaries contained follicles of all stages (primordial, primary, secondary, and antral) as well as CL. Follicles showed typical histology (Figure 5). Morphometric analysis confirmed that *Grem2*$^{-/-}$ ovaries from mice aged 7–9 months of age contained similar numbers of primordial follicles but statistically more primary follicles ($P < 0.05$) than the WT (Figure 5E). In addition, *Grem2*$^{-/-}$ had statistically fewer antral follicles ($P < 0.05$) and CL ($P < 0.01$) (Figure 5E). There were no significant changes in the number of atretic follicles.

A histologic pathology was identified in 75% of *Grem2*$^{-/-}$ ($n = 4$) 6-month-old ovaries, which contained unusually large patches of PAS+ regions. Six-month-old WT ovaries ($n = 4$) showed only minimal patches (Figure 5C and D). These large patches of PAS+ cells have been described as multinucleated macrophage giant cells, which are typically only present in ovaries from aged mice and mostly absent from mice less than 7 months of age [33]. By immunohistochemistry, these cells were positive for the mouse macrophage marker F4/80 (Figure 5F and G). Previous studies indicate that in aged mouse ovaries, the presence of macrophage giant cells is associated with increased fibrosis and inflammation [33]. To identify if *Grem2*$^{-/-}$ ovaries have increased fibrosis, 6-month-old ovary sections were stained with picrosirius red (PSR), an indicator of fibrous collagen in the ovary [33]. However, a similar level of PSR staining was observed between genotypes, indicating similar levels of fibrous collagen in the ovaries (data not shown). As a prior study of *Grem2*$^{-/-}$mice also identified increases in inflammatory markers in the heart after myocardial infarction (MI), including *Bmp2*, tumor necrosis factor alpha (*Tnf*), and e-selectin (*Sele*) [34], we analyzed potential upregulation of these genes in 6-month-old ovaries from WT and *Grem2*$^{-/-}$ by qPCR but no differences in expression of these genes were found (Supplementary Table S2).

Disruptions to the estrous cycle could be due to HPO axis dysfunction, but there is limited information regarding a role for

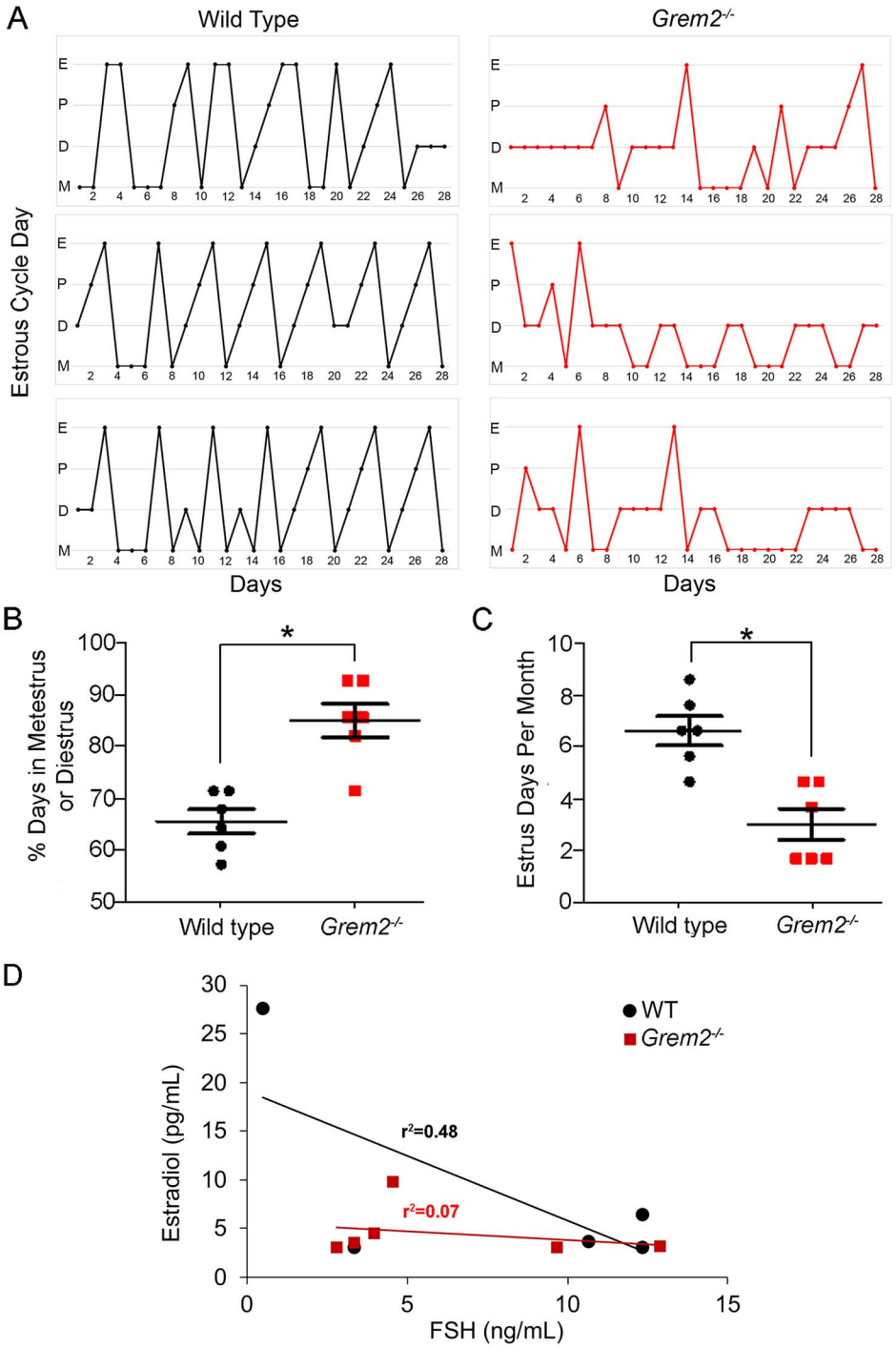

Figure 3. *Grem2*$^{-/-}$ mice have irregular estrous cycles. (A) Three typical estrous cycles for each genotype are shown for 6-month-old WT (black) and *Grem2*$^{-/-}$ (red) mice from a total of $n = 6$ mice per genotype. Estrous cycle day is indicated on the *y*-axis as estrus (E), proestrus (P), diestrus (D), and metestrus (M) for both genotypes. (B) Percentage of time in metestrus and diestrus, and (C) number of days in estrus for 6-month-old WT ($n = 6$) and *Grem2*$^{-/-}$ ($n = 6$) for a 1-month period. $^*P < 0.05$. (D) Linear regression of serum estradiol (pg/mL) and FSH (ng/mL) in WT (shown as black circles) ($n = 5$) ($r^2 = 0.48$) and *Grem2*$^{-/-}$ (shown as red squares) ($n = 6$) at 6 months of age shows lack of correlation between serum estradiol and FSH in diestrous stage *Grem2*$^{-/-}$ mice ($r^2 = 0.07$).

Grem2 in the HPO axis outside of its role in the ovary, even though BMP4 is known to be important in mouse pituitary development [35] and may regulate FSH in gonadotropes [36, 37]. *Grem2* is expressed in the brain [1], but hypothalamic expression has not been published [38]. In adult WT mice, by qPCR, *Grem2* was undetectable in the pituitary but expressed in the hypothalamus (Figure 6A). To further determine how the HPO axis may be disrupted, we measured ovarian expression of the inhibin/activin genes, which play a role in HPO negative feedback and suppression of FSH. Transcript levels of *Inha*, *Inhba*, and *Inhbb* are significantly increased in 6-month-old

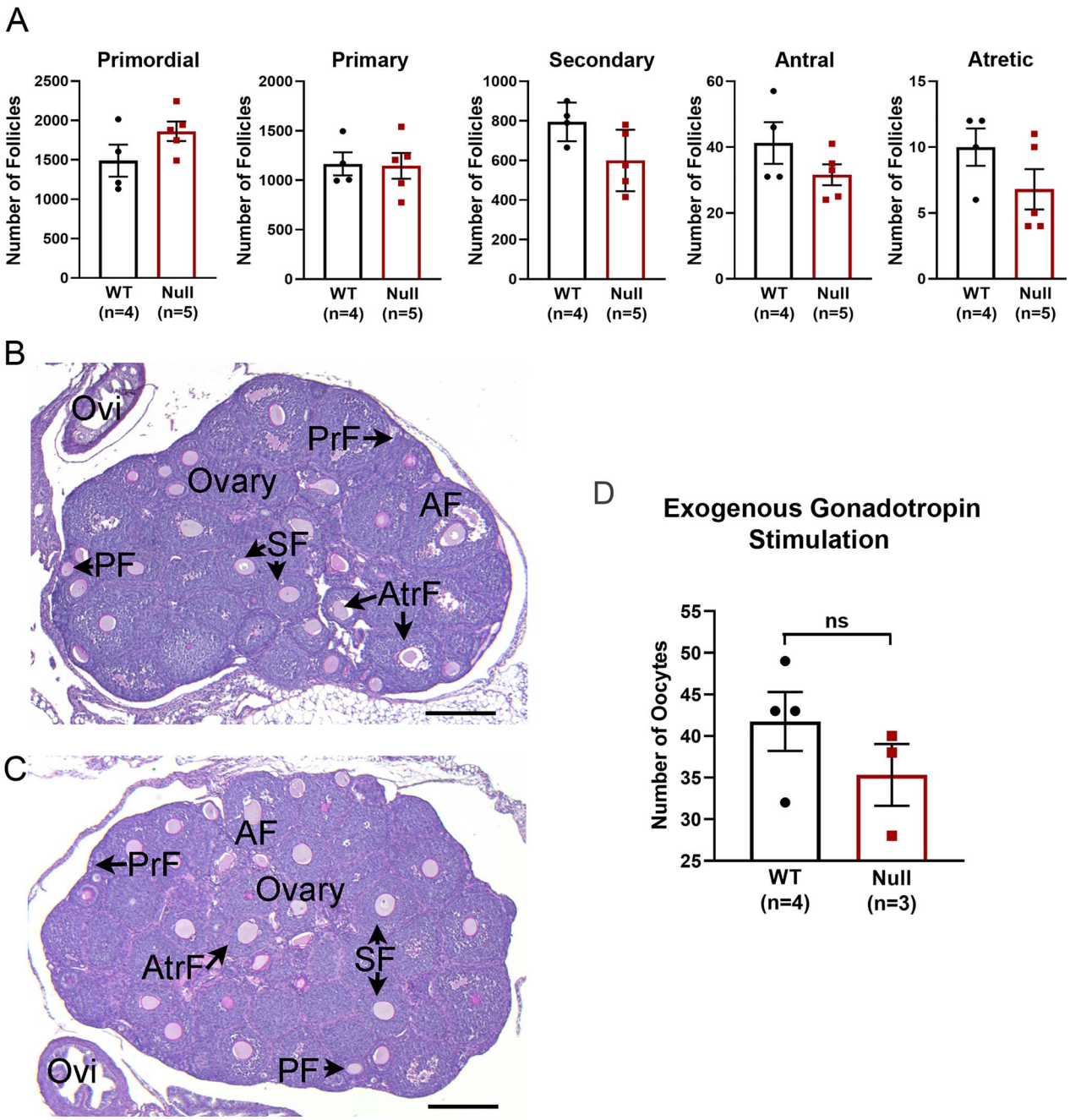

Figure 4. *Grem2*$^{-/-}$ ovaries show normal follicle morphometrics and response to exogenous gonadotropin stimulation prior to sexual maturity. (A) Morphometric assessment of follicle numbers in sexually immature mice (3-weeks old). Shown are mean ± s.e.m. of follicle counts obtained from independent ovaries of WT ($n = 4$; shown as black circles) and *Grem2*$^{-/-}$ ("Null"; $n = 5$; shown as red squares) mice. No differences in means were detected in any follicle stage by Student's *t*-test between genotypes. (B) Representative PAS histology for a 3-week-old WT ovary showing primordial follicles (PrF), primary follicles (PF), SF, and antral follicles (AF). The oviduct (OVI) is also indicated. (C) Representative PAS histology for a 3-week-old Grem2$^{-/-}$ with similar follicle stages as the WT. Scale bar in B and C is 200 µm. (D) The mean number of eggs (±s.e.m) collected from the oviduct ampulla following exogenous gonadotropin stimulation is shown for 5-week-old WT ($n = 4$) and *Grem2*$^{-/-}$ ("Null"; $n = 3$) females. Data from individual animals are shown as black circles (WT) or red squares (*Grem2*$^{-/-}$). Statistical analysis by Student's *t*-test showed no difference in means (ns) between groups.

Grem2$^{-/-}$ ovaries compared with WT ($P < 0.05$) (Supplementary Table S2). Other ovarian markers showed no difference between genotypes, including genes expressed in oocytes (*Bmp15*, *Gdf9*), granulosa cells (*Bmp2*, *Cype19a1*, *Fshr*, *Kitl1/2*), or thecal cells (*Bmp4*) (Supplementary Table S2).

Because of its role as a marker of the ovarian reserve [39–41], we measured serum levels of AMH. *Grem2*$^{-/-}$ mice showed significantly reduced levels of AMH at 6 months of age ($P < 0.01$) (Figure 6B). As AMH is most highly secreted from granulosa cells of growing follicles, AMH immunoreactivity in individual follicles was quantified by immunofluorescence (Figure 7). When plotted by mean fluorescent intensity versus follicle stage, AMH immunoreactivity was significantly reduced in *Grem2*$^{-/-}$ preantral follicles mice compared with WT follicles (Figure 7B), and specifically, in

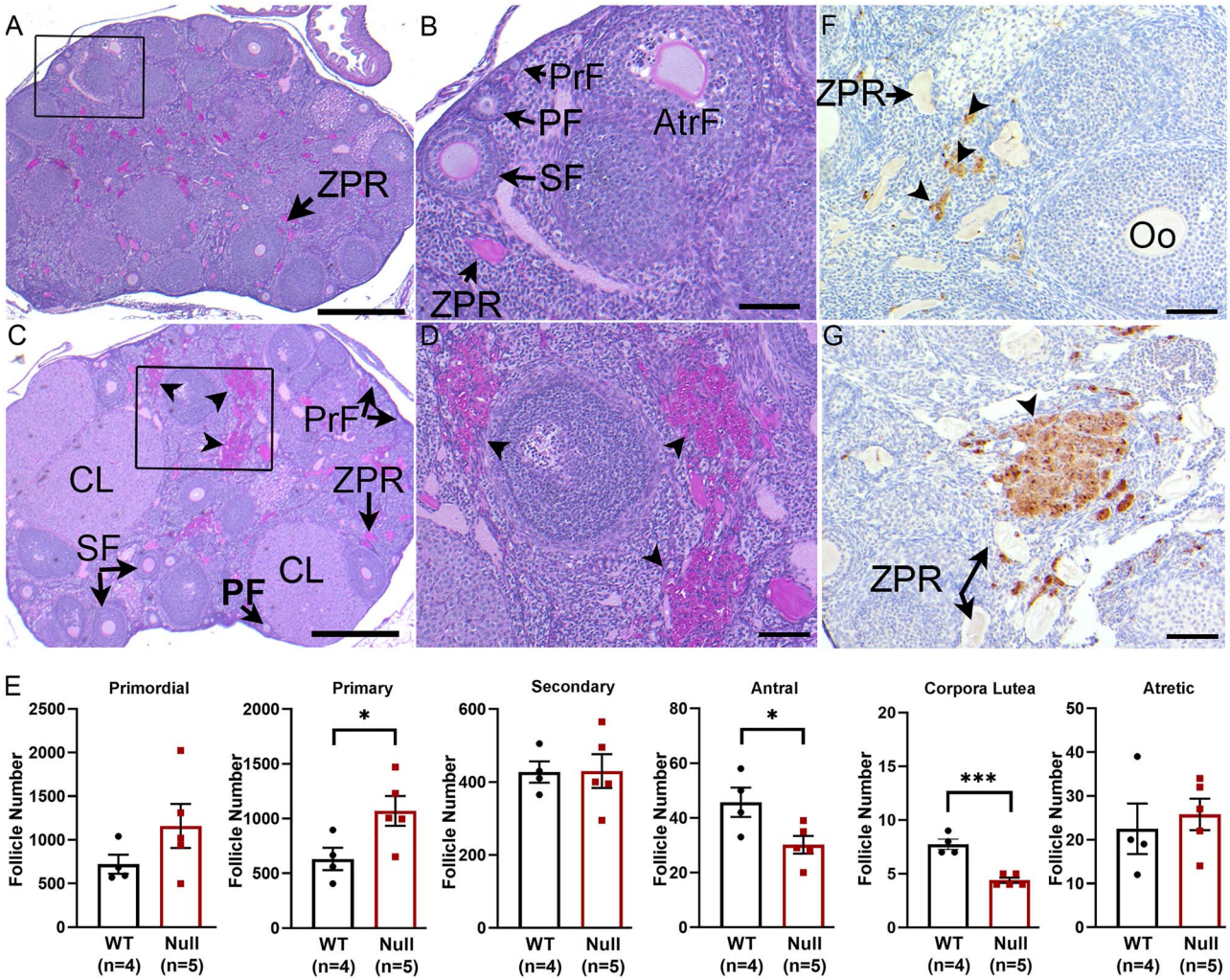

Figure 5. Older adult *Grem2*$^{-/-}$ ovaries have a normal ovarian reserve and CL, but evidence of pathologic macrophage infiltration at 6 months of age. (A, B) Representative PAS histology of a WT ovary at 6 months of age showing all stages of follicles and oocyte remnants (ZPR) within the interior of the ovary, which is typical in this strain of mice. Area boxed in (A) is shown at a higher magnification in panel B. (B) Boxed area from panel (A) showing primordial follicles (PrF), primary follicles (PF), SF, ZPR, and an atretic follicle (Atr) at higher magnification for the representative WT ovary. (C) Representative PAS histologic section of an ovary from a 6-month-old *Grem2*$^{-/-}$ mouse. All follicle stages are present including CL. Boxed area in panel C is shown as higher magnification images in panel D. Arrowheads in panels C and D indicate large patches of PAS+ cells that are distinct from PAS+ ZPRs. (E) Quantification of follicle numbers (mean ± s.e.m) in WT ($n=4$) and *Grem2*$^{-/-}$ ("Null") ovaries ($n=5$) at 7–9 months of age. Statistically significant differences between means were seen for primary follicles (increased; $^{*}P<0.05$), antral (decreased; $^{*}P<0.05$), and corporal lutea (decreased; $^{***}P<0.001$) by Student's *t*-test between WT and Null. (F) Anti-F4/80 immunostaining in a representative 6-month-old WT ovary showing the typical pattern of single positive cells (arrowheads; brown stain) scattered within the stroma, theca, and CL. (G) Representative 6-month-old *Grem2*$^{-/-}$ ovary at the same magnification as panel F showing regions of F4/80 positive immunoreactivity (arrowheads; brown stain) in areas that are larger and less dispersed as well as an F4/80 negative ZPR (arrows). Slides are counterstained in hematoxylin (blue). Scale bar in panels A, C, 200 µm; panel B, D,F, G, scale bar 50 µm.

secondary stage follicles (Figure 7D). This supports the premise that the reduction in serum AMH is caused by a loss of AMH production in the granulosa cells that typically produce it and not due to the loss of follicles themselves.

GREM2 has a rare variant in patient samples of POI

Published cohorts of 106 POI patient samples that had undergone WES were queried for nonsynonymous and splice site variants in GREM2 [24, 25]. One individual contained a novel nonsynonymous heterozygous variant in *GREM2*, c.C356T:p.S119F in exon 2. This patient had a normal puberty but was diagnosed at age 27 with primary amenorrhea with absent ovaries during ultrasound examination and FSH (73 mIU/mL; normal range, 3.5–12.5 mIU/mL), estradiol (10 pg/mL; normal range 13–166 pg/mL), and AMH (0.05 ng/mL, normal range, 0.5–3.8 ng/mL) [24] in the menopausal range. This variant was not present in The Genome Aggregation Database (gnomAD) or other databases. We further modeled the location of this variant based on the published crystal structure of GREM2 with GDF5 [4]. The S119F variant lies in the interface of the interaction domain between antagonist and ligand (Figure 8), which has been shown to be key region required for robust BMP antagonism [4].

Discussion

Because of their roles as powerful developmental morphogens and regulators of adult tissue homeostasis, BMP activity is under strict biologic control. One mechanism for their regulation is through

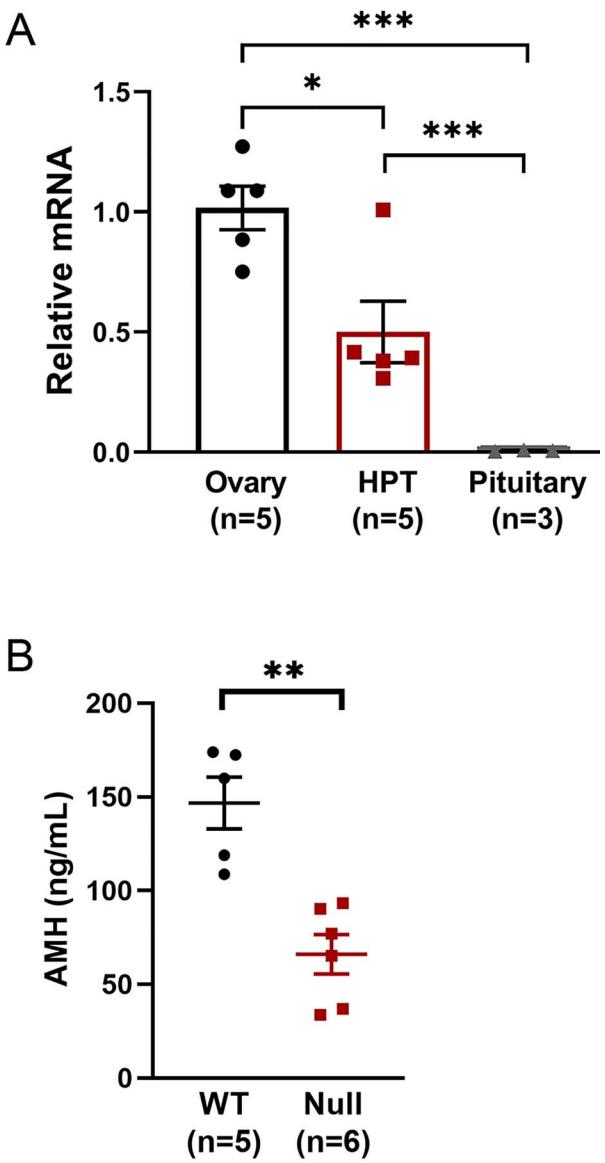

Figure 6. *Grem2* is expressed in WT ovary and hypothalamus but not pituitary and *Grem2*$^{-/-}$ females show a significant decrease in serum AMH. (A) Relative mRNA expression levels by qPCR for *Grem2* in the adult WT mouse ovary (black circles; $n=5$), hypothalamus (red squares; $n=5$), and pituitary (grey triangles; $n=3$). qPCR was analyzed by the ΔΔCT method normalized to *Gapd*; data are shown relative to the level of *Grem2* in the ovary; $^{*}P<0.05$ by one-way analysis of variance with Bonferroni's Multiple Comparison Test. (B) Serum AMH levels in diestrous stage 6-month-old WT (black circles; $n=5$) and *Grem2*$^{-/-}$ (red squares; $n=6$) as measured by ELISA (ng/mL). Shown are mean ± s.e.m. Data were log transformed prior to statistical analysis by Mann–Whitney U test, $^{**}P<0.01$.

production of extracellular binding proteins, including GREM2, which, when bound to BMPs, disrupts the ability of the ligand to form the ternary signaling receptor complex. GREM2 exists as a stable nondisulfide bonded dimer with binding affinities for BMP2 and BMP4 in the nanomolar range [1, 4, 42]. Additionally, GREM2 binds and inhibits AMH, another member of the TGFβ family, in in-vitro assays [5]. A previous mouse KO of *Grem2* was published as part of a high-throughput KO phenotyping program by Lexicon Pharmaceuticals that included fertility assays. These assays were performed from ages 8–16 weeks using two homozygous KO females mated to a WT male [43]. Lexicon's *Grem2*$^{-/-}$ line showed defects related to small and malformed upper and lower mandibular incisors [10]. No fertility defects were noted, though the fertility screen may not have had sufficient depth to identify changes in fecundity beyond overt sterility, particularly for those that arise due to aging. That model was unavailable, so we developed a new *Grem2*$^{-/-}$ mouse model using CRISPR/Cas9 gene targeting to delete the entire coding exon. This new mouse model phenocopies the Lexicon deletion with respect to dental defects, even though the genetic background is dissimilar [inbred C57/Bl6 (albino) versus mixed hybrid in our study], suggesting a robust phenotype in tooth development resulting from loss of *Grem2*.

Unlike homozygous mutations in *Grem1*, which are perinatal lethal [21, 44], *Grem2*$^{-/-}$ mice are viable, but females are subfertile. Overall litter production in *Grem2*$^{-/-}$ females was reduced throughout the reproductive lifespan and slightly worsens after 6 months of age. The overall change in litter production primarily results from irregular estrous cycles. As *Grem2* is widely expressed and transcripts have been identified in the mouse ovary, brain, and uterus [1], it is currently unclear if the changes in cyclicity are due intra-ovarian defects, defects in other tissues, or most likely, a combination of both. Within the mouse ovary, *Grem2* is expressed in granulosa cells and is upregulated in response to gonadotropin stimulation [1, 21, 45]. We did not detect *Grem2* in the adult WT mouse pituitary by qPCR, but transcripts were amplified from the hypothalamus. The relative contribution of intra-ovarian defects versus potential hypothalamic defects remains to be determined and would require generation of a conditional allele for *Grem2* for cell-specific deletion. Interestingly, the AMH receptor (*Amhr*) has been reported in a subset of gonadotropin releasing hormone (GnRH) neurons within the hypothalamus and at least one study has shown that AMH potently activates GnRH neuron firing and GnRH-dependent LH pulsatility and secretion [46]. Clinically, AMH is used to predict response to ovarian stimulation owing to the well documented correlation with the ovarian reserve [47, 48]. If GREM2 binds to and regulates AMH as previously suggested [5], then it is plausible that GnRH neuronal activity may be disrupted in *Grem2*$^{-/-}$ females and contributes to the observed reproductive defects. Such studies require more precise measurements of LH pulse generation, rather than the steady state (e.g., diestrus) levels reported here.

The role of GREM2 in the ovary in vivo is not well characterized. Previous studies suggest GREM2 functions in embryonic human ovary development, as its expression increases between 8–11 weeks and 14–16 weeks gestation; this corresponds to the timing of postmigratory germ cell proliferation and entry into meiosis I, respectively, and demonstrates that GREM2 partially antagonizes BMP4-induced gene expression [12]. Other studies have shown that the treatment of organ cultures of rat ovaries with GREM2 reverses the ability of AMH to suppress primordial follicle activation [5]. Surprisingly, we found ovaries from sexually immature *Grem2*$^{-/-}$ mice that contain equivalent numbers of primordial follicles as the WT control mice. This suggests that *Grem2* may not play a significant role in the formation of the ovarian reserve in mice or potentially and that developmental changes to the ovarian reserve resolve to WT levels during the first wave of folliculogenesis [49]. This differs from mice homozygous null for *Grem1*, which have decreased numbers of germ cells and primordial follicles at birth [21]. Alternatively, the lack of defects in 3-week-old *Grem2*$^{-/-}$ ovaries may indicate that the loss of *Grem2* in the embryo or postnatally is compensated for by

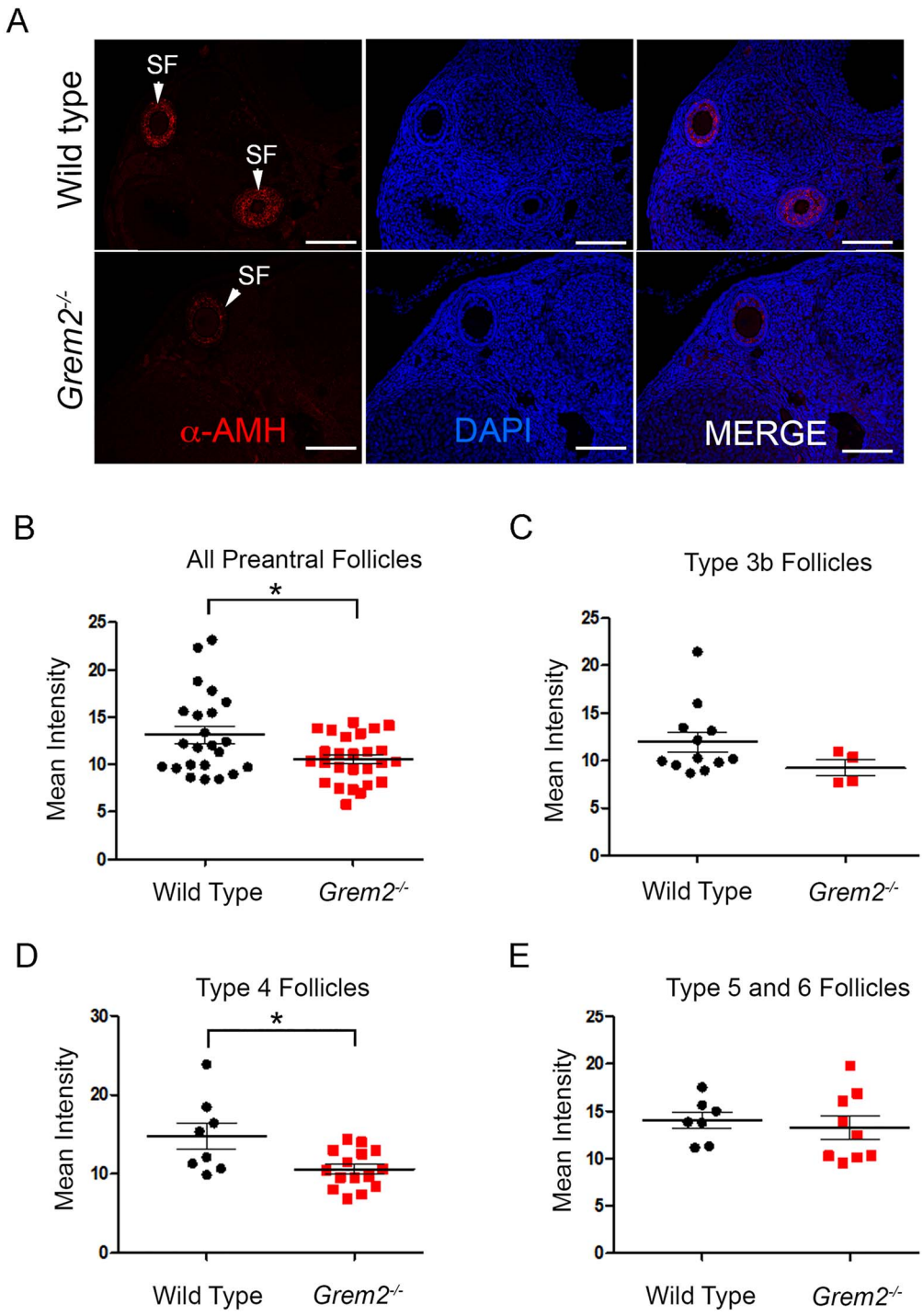

Figure 7. Growing preantral follicles from *Grem2*$^{-/-}$ mice produce reduced levels of AMH. Ovary sections from 6-month-old WT and *Grem2*$^{-/-}$ mice were analyzed for AMH immunoreactivity by immunofluorescence microscopy (red); DAPI (blue) was used to stain nuclei (A). Arrowheads indicate SF. Scale bars, 100 µm ($n=3$ per genotype). Data were analyzed by classifying follicles as all preantral follicles (B) or by individual types (follicle stages 3b, 4, 5, and 6) (C, D, and E). The group of "all preantral follicles" (panel B) showed significantly lower levels of expression in the *Grem2*$^{-/-}$ mice, as did individual type 4 follicles (panel D); $^{*}P < 0.05$.

another BMP antagonist, such as *Grem1*. Functional redundancy between *Grem2* and *Grem1* has been hypothesized [5, 21], but not yet demonstrated in vivo.

Histologic and morphometric analysis of ovaries from adult *Grem2*$^{-/-}$ showed all stages of follicle growth, including primordial follicles, and initially *Grem2*$^{-/-}$ females produced normal-sized litters and ovaries responded similar to WT in "superovulation" protocols; at later ages, there was a minor decrease in litter sizes. This suggests an intra-ovarian defect in older mice. While the mean diestrus serum levels of estradiol and FSH were similar between

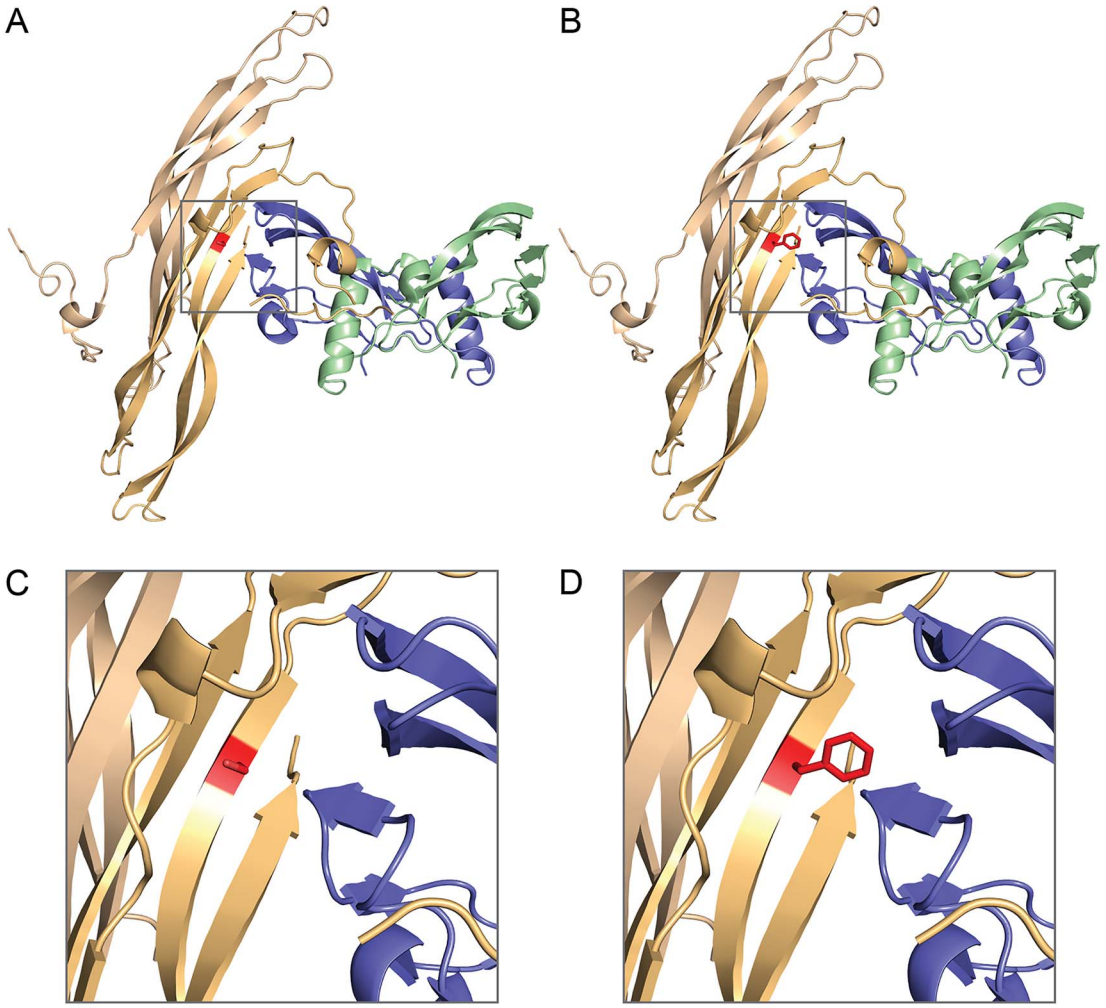

Figure 8. Model of the GREM2 variant S119F with the ligand GDF5. (A) Structure of GREM2 (monomers in pale orange and tan) in complex with GDF5 (monomers in slate and pale green) with S119 shown in red, PDB ID: 5HK5 [4]. (B) Structure of GREM2-GDF5 with S119 mutated to F119, with the most probable rotomer shown in red. (C) Zoomed in view of panel A, focusing on the S119 residue and its local interactions. (D) Zoomed in view of panel B, focusing the F119 residue and its local interactions.

WT and *Grem2*$^{-/-}$ mice, the well-known correlation between estradiol and FSH was altered in *Grem2*$^{-/-}$ females. In WT rodents, at metestrus and diestrus, low but rising levels of estradiol from granulosa cells negatively regulate the production of FSH by suppressing hypothalamic secretion of gonadotropin releasing hormone [50, 51]. Furthermore, circulating levels of inhibin suppress FSH production from the pituitary [52, 53]. In *Grem2*$^{-/-}$ ovaries, genes required to make inhibin and activin (*Inha, Inhba, Inhbb*) were upregulated in adults, which may further contribute to changes to reproductive cyclicity. Inhibin A and inhibin B production in granulosa cells varies with estrous cycle stage [53] and a more detailed analysis of circulating inhibin levels, intra-ovarian activin levels, as well as FSH and LH production and secretion during the different stages of the estrous cycle may help to resolve these issues in *Grem2*$^{-/-}$ mice.

In *Grem2*$^{-/-}$ ovaries, there was a reduction in granulosa cell production of AMH, which is reflected in the loss of serum AMH. *Amh* is most abundantly produced from growing preantral follicles [54, 55] and it is downregulated in FSH-responsive antral follicles except in cumulus cells [56, 57]. *Grem2*$^{-/-}$ females have increases in primary follicles and similar numbers of secondary follicles (SF) compared with their WT littermates—the follicle stages that should produce the most AMH; therefore, reductions in serum AMH in *Grem2*$^{-/-}$ are driven by the lack of production in small follicles, not loss of the follicle stages themselves. As cumulus cells make up a minor proportion of antral follicles compared with the number of mural granulosa cells, the minor decrease in the antral follicle count in *Grem2*$^{-/-}$ is likely not sufficient to drive the large reductions in serum AMH levels. Loss of AMH in *Grem2*$^{-/-}$ ovaries could be directly or indirectly related to changes in BMP signaling, as the regulation of *Amh* by various growth factor pathways during preantral folliculogenesis is not fully understood [58]. Loss of *Grem2* should increase local BMP signaling (i.e., lead to a gain-of-function in BMP signaling). In this scenario, if loss of AMH is directly related to increased BMP signaling in the *Grem2*$^{-/-}$ model, this would contradict in vitro studies showing BMP2, BMP4, or BMP15 stimulate AMH expression [59–61]. An alternative explanation would be that there may be species-specific differences in regulation of AMH, with

some BMP able to downregulate *Amh* in mice. It is also possible that the reductions in AMH production in *Grem2*$^{-/-}$ mice are unrelated to changes in BMP signaling but occur through additional changes to other signaling pathways that remain to be determined.

As AMH is widely used as a clinical marker of the ovarian reserve [39–41], it was surprising to find that while serum and follicle AMH production is reduced in *Grem2*$^{-/-}$; there were no changes to the numbers of primordial follicles, even up to 9 months of age. This likely reflects the complexities that regulate primordial follicle quiescence and activation [62–65]. Reductions of AMH in *Grem2*$^{-/-}$ are possibly balanced by expression/upregulation of local factors that regulate the stability of the primordial follicle pool. For instance, the increased number of growing, primary follicles in *Grem2*$^{-/-}$, may reflect reductions in AMH, a negative regulator of primordial follicle recruitment, alongside gain-of-function in BMPs, which serves to promote the primordial to primary transition [13, 66]. Even so, the number of growing primary follicles only increased by ~2 fold in *Grem2*$^{-/-}$, and this change may be insufficient to significantly deplete the stock of primordial follicles. Understanding the interplay of factors in the *Grem2*$^{-/-}$ model that regulate the dynamics of follicle recruitment may also lead to the discovery of additional markers of the ovarian reserve and the complex signals that balance primordial follicle quiescence and activation.

While adult ovaries from *Grem2*$^{-/-}$ appear to contain the full range of expected follicle stages, including primordial follicles and CLs, there was an obvious and pathologic accumulation of large patches of F4/80+ multinucleated macrophage giant cells that were not present in *Grem2*$^{-/-}$ovaries at 3 weeks or 3 months of age (data not shown). The significance of macrophage giant cells is unknown, but ovaries from aged WT female mice (14–17 months of age) accumulate the areas of fibrotic tissue consistent with chronic inflammation and macrophage giant cells, which are generally absent in WT ovaries from mice less than 7 months of age (CD1 and CB6F1 strains) [33]. Thus, *Grem2*$^{-/-}$ ovaries have one hallmark of premature aging, but without significant changes in fibrosis. The presence of large patches of F4/80+ macrophages suggests an increase in tissue inflammation; this is similar to a previous study of *Grem2*$^{-/-}$ in the heart during recovery from MI [34]. Following MI, *Grem2*$^{-/-}$ hearts show excessive inflammation, including increases in F4/80+ macrophages and poorer functional outcomes as result of overactive BMP signaling, which can be rescued by intraperitoneal administration of recombinant GREM2 [34]. Furthermore, a BMP pro-inflammatory cascade has been suggested in other diseases, including chronic inflammatory arthritis and atherosclerosis, though in other diseases BMP signaling is anti-inflammatory [67, 68]. How the loss of *Grem2* affects the balance of TGFβ superfamily signaling, including AMH and BMPs, within the ovary remains to be determined. As AMH has reduced expression in follicles of *Grem2*$^{-/-}$ ovaries, inter- and intrafollicle BMP signaling may predominate over AMH, promoting macrophage recruitment or differentiation, disrupting ovarian function, and possibly altering feedback within the HPO axis.

A number of studies implicate altered BMP signaling with POI in women. This includes genetic variants in ligands (*BMP15*) [69, 70], promoters (*BMP15*) [71], receptors (*BMPR1A* and *BMPR1B*) [72], and antagonists (*GREM1)* [11], but not previously for *GREM2*. How these variants contribute to POI in unknown. As each of these genes is expressed in multiple organs within the HPO axis [36, 73–76], alterations in their activity and the resulting development of POI could occur at multiple levels. The patient with the heterozygous S119F-GREM2 variant is 27-year-old patient with POI previously characterized with a homozygous variant in the mitochondrial histidyl-tRNA synthetase gene (*HARS2)* (c.1010A > G) [24]. While this variant in HARS2 is damaging by computational analysis, it has not been shown to be pathogenic and further studies will be needed to determine which variant contributed to POI in this patient. Structure–function studies of GREM2 with GDF5 indicate that GREM2 forms alternating higher form stable aggregates with its ligands, which is unique among BMP antagonists [4]. The S119F mutation lies within the interface between GREM2 and GDF5, though how this mutation affects antagonism is not known. Mechanistically, GREM2 wraps around the BMP signaling molecule, occluding both the type I (located at the concave dimer interface) and type II (at the convex surface of the ligand) binding sites needed for signaling [4]. The side chain of the S119 residue points directly into one of the primary binding interfaces of GDF5, specifically the one that impairs binding of GDF5 to the type II BMP receptors. Previous mutational work has demonstrated that this section of GREM2 is particularly key to robust BMP inhibition and sensitive to mutational disruption [4]. Additionally, modeling S119 with a phenylalanine showed a significant steric clash occurred with both the ligand and residues of GREM2 important for GDF5 binding. Thus, the S119F mutation likely would interfere with ligand binding and weaken GREM2 antagonism, potentially leading to a gain-of-function in BMP or AMH signaling. The genetic variants found for *BMPR1A* (*ALK3*) and *BMPR1B* (*ALK6*) are located within the kinase domain of the receptors; the BMPR1A p.Arg442His variant inhibits receptor activation and was discovered in a patient with menarche at 14 years and amenorrhea 1 year later [72]. The BMPR1B p.Phe272Leu variant shows constitutive activation when tested in vitro, and was discovered in a patient with secondary amenorrhea at age 27 [72]. Thus, both loss-of-function and gain-of-function mutations that alter BMP signaling may drive POI. Additional structure–function studies will be required to understand how *GREM2*, c.C356T:p.S119F alters BMP or AMH signaling and its consequences on HPO function.

Data availability

The data underlying this article will be shared on reasonable request to the corresponding author.

Authors' contributions

R.T.R. performed experiments, analyzed data, interpreted results, and wrote portions of the manuscript; B.K.P. performed experiments, analyzed data, interpreted results, and assisted with manuscript preparation and revision; H.S.T. performed experiments; S.M.B. performed experiments and analyzed data; G.G. performed experiments related to protein modeling; R.J. performed experiments and analyzed data; A.R. provided data and interpreted results; T.T. analyzed and interpreted results; and S.A.P. conceived the study, performed experiments, analyzed data, interpreted results, and wrote the manuscript with input from all authors. All authors provided critical feedback and edited the manuscript.

Supplementary material

Supplementary material is available at *BIOLRE* online.

Acknowledgments

We thank Ramya Masand, MD (Baylor College of Medicine) for histology assessment and Shailaja K. Mani, PhD (Baylor College of Medicine) for help with mouse hypothalamic dissections and discussion on regulation of the HPO axis. We thank Ernesto Salas for additional assistance with genotyping and maintenance of the *Grem2* colony.

Conflict of interest

The authors have nothing to declare.

References

1. Sudo S, Avsian-Kretchmer O, Wang LS, Hsueh AJ. Protein related to DAN and cerberus is a bone morphogenetic protein antagonist that participates in ovarian paracrine regulation. *J Biol Chem* 2004; **279**: 23134–23141.
2. Minabe-Saegusa C, Saegusa H, Tsukahara M, Noguchi S. Sequence and expression of a novel mouse gene PRDC (protein related to DAN and cerberus) identified by a gene trap approach. *Dev Growth Differ* 1998; **40**:343–353.
3. Gazzerro E, Canalis E. Bone morphogenetic proteins and their antagonists. *Rev Endocr Metab Disord* 2006; **7**:51–65.
4. Nolan K, Kattamuri C, Rankin SA, Read RJ, Zorn AM, Thompson TB. Structure of Gremlin-2 in complex with GDF5 gives insight into DAN-family-mediated BMP antagonism. *Cell Rep* 2016; **16**:2077–2086.
5. Nilsson EE, Larsen G, Skinner MK. Roles of gremlin 1 and gremlin 2 in regulating ovarian primordial to primary follicle transition. *Reproduction* 2014; **147**:865–874.
6. Kaminski A, Bogacz A, Uzar I, Czerny B. Association between GREM2 gene polymorphism with osteoporosis and osteopenia in postmenopausal women. *Eur J Obstet Gynecol Reprod Biol* 2018; **228**:238–242.
7. Muller II, Melville DB, Tanwar V, Rybski WM, Mukherjee A, Shoemaker MB, Wang WD, Schoenhard JA, Roden DM, Darbar D, Knapik EW, Hatzopoulos AK. Functional modeling in zebrafish demonstrates that the atrial-fibrillation-associated gene GREM2 regulates cardiac laterality, cardiomyocyte differentiation and atrial rhythm. *Dis Model Mech* 2013; **6**:332–341.
8. Mostowska A, Biedziak B, Zadurska M, Bogdanowicz A, Olszewska A, Cieslinska K, Firlej E, Jagodzinski PP. GREM2 nucleotide variants and the risk of tooth agenesis. *Oral Dis* 2018; **24**:591–599.
9. Cheung CL, Lau KS, Sham PC, Tan KC, Kung AW. Genetic variants in GREM2 are associated with bone mineral density in a southern Chinese population. *J Clin Endocrinol Metab* 2013; **98**:E1557–E1561.
10. Vogel P, Liu J, Platt KA, Read RW, Thiel M, Vance RB, Brommage R. Malformation of incisor teeth in Grem2−/− mice. *Vet Pathol* 2014; **52**:224–229.
11. Patino LC, Beau I, Carlosama C, Buitrago JC, Gonzalez R, Suarez CF, Patarroyo MA, Delemer B, Young J, Binart N, Laissue P. New mutations in non-syndromic primary ovarian insufficiency patients identified via whole-exome sequencing. *Hum Reprod* 2017;**32**:1–9.
12. Bayne RA, Donnachie DJ, Kinnell HL, Childs AJ, Anderson RA. BMP signalling in human fetal ovary somatic cells is modulated in a gene-specific fashion by GREM1 and GREM2. *Mol Hum Reprod* 2016; **22**:622–633.
13. Durlinger AL, Gruijters MJ, Kramer P, Karels B, Ingraham HA, Nachtigal MW, Uilenbroek JT, Grootegoed JA, Themmen AP. Anti-Mullerian hormone inhibits initiation of primordial follicle growth in the mouse ovary. *Endocrinology* 2002; **143**:1076–1084.
14. Ran FA, Hsu PD, Wright J, Agarwala V, Scott DA, Zhang F. Genome engineering using the CRISPR-Cas9 system. *Nat Protoc* 2013; **8**:2281–2308.
15. Bassett AR, Tibbit C, Ponting CP, Liu JL. Highly efficient targeted mutagenesis of Drosophila with the CRISPR/Cas9 system. *Cell Rep* 2013; **4**:220–228.
16. Byers SL, Wiles MV, Dunn SL, Taft RA. Mouse estrous cycle identification tool and images. *PLoS One* 2012; **7**:e35538.
17. Pangas SA, Jorgez CJ, Tran M, Agno J, Li X, Brown CW, Kumar TR, Matzuk MM. Intraovarian activins are required for female fertility. *Mol Endocrinol* 2007; **21**:2458–2471.
18. Tilly JL. Ovarian follicle counts–not as simple as 1, 2, 3. *Reprod Biol Endocrinol* 2003; **1**:11.
19. Whitcomb BW, Schisterman EF. Assays with lower detection limits: implications for epidemiological investigations. *Paediatr Perinat Epidemiol* 2008; **22**:597–602.
20. Middlebrook BS, Eldin K, Li X, Shivasankaran S, Pangas SA. Smad1-Smad5 ovarian conditional knockout mice develop a disease profile similar to the juvenile form of human granulosa cell tumors. *Endocrinology* 2009; **150**:5208–5217.
21. Myers M, Tripurani SK, Middlebrook B, Economides AN, Canalis E, Pangas SA. Loss of gremlin delays primordial follicle assembly but does not affect female fertility in mice. *Biol Reprod* 2011; **85**:1175–1182.
22. Pedersen T, Peters H. Proposal for a classification of oocytes and follicles in the mouse ovary. *J Reprod Fertil* 1968; **17**:555–557.
23. Livak KJ, Schmittgen TD. Analysis of relative gene expression data using real-time quantitative PCR and the 2(-Delta Delta C(T)) method. *Methods* 2001; **25**:402–408.
24. Yang X, Touraine P, Desai S, Humphreys G, Jiang H, Yatsenko A, Rajkovic A. Gene variants identified by whole-exome sequencing in 33 French women with premature ovarian insufficiency. *J Assist Reprod Genet* 2019; **36**:39–45.
25. Desai S, Wood-Trageser M, Matic J, Chipkin J, Jiang H, Bachelot A, Dulon J, Sala C, Barbieri C, Cocca M, Toniolo D, Touraine P et al. MCM8 and MCM9 nucleotide variants in women with primary ovarian insufficiency. *J Clin Endocrinol Metab* 2017; **102**:576–582.
26. Richards S, Aziz N, Bale S, Bick D, Das S, Gastier-Foster J, Grody WW, Hegde M, Lyon E, Spector E, Voelkerding K, Rehm HL et al. Standards and guidelines for the interpretation of sequence variants: a joint consensus recommendation of the American College of Medical Genetics and Genomics and the Association for Molecular Pathology. *Genet Med* 2015; **17**:405–424.
27. Genomes Project C, Auton A, Brooks LD, Durbin RM, Garrison EP, Kang HM, Korbel JO, Marchini JL, McCarthy S, McVean GA, Abecasis GR. A global reference for human genetic variation. *Nature* 2015; **526**:68–74.
28. Lek M, Karczewski KJ, Minikel EV, Samocha KE, Banks E, Fennell T, O'Donnell-Luria AH, Ware JS, Hill AJ, Cummings BB, Tukiainen T, Birnbaum DP et al. Analysis of protein-coding genetic variation in 60,706 humans. *Nature* 2016; **536**:285–291.
29. Sherry ST, Ward MH, Kholodov M, Baker J, Phan L, Smigielski EM, Sirotkin K. dbSNP: the NCBI database of genetic variation. *Nucleic Acids Res* 2001; **29**:308–311.
30. Myers M, Mansouri-Attia N, James R, Peng J, Pangas SA. GDF9 modulates the reproductive and tumor phenotype of female inha-null mice. *Biol Reprod* 2013; **88**:86.
31. Pangas SA, Li X, Umans L, Zwijsen A, Huylebroeck D, Gutierrez C, Wang D, Martin JF, Jamin SP, Behringer RR, Robertson EJ, Matzuk MM. Conditional deletion of Smad1 and Smad5 in somatic cells of male and female gonads leads to metastatic tumor development in mice. *Mol Cell Biol* 2008; **28**:248–257.
32. Reed DR, Bachmanov AA, Tordoff MG. Forty mouse strain survey of body composition. *Physiol Behav* 2007; **91**:593–600.
33. Briley SM, Jasti S, McCracken JM, Hornick JE, Fegley B, Pritchard MT, Duncan FE. Reproductive age-associated fibrosis in the stroma of the mammalian ovary. *Reproduction* 2016; **152**:245–260.
34. Sanders LN, Schoenhard JA, Saleh MA, Mukherjee A, Ryzhov S, McMaster WG Jr, Nolan K, Gumina RJ, Thompson TB, Magnuson MA, Harrison DG, Hatzopoulos AK. BMP antagonist gremlin 2 limits inflammation after myocardial infarction. *Circ Res* 2016; **119**:434–449.
35. Takuma N, Sheng HZ, Furuta Y, Ward JM, Sharma K, Hogan BL, Pfaff SL, Westphal H, Kimura S, Mahon KA. Formation of Rathke's pouch requires dual induction from the diencephalon. *Development* 1998; **125**:4835–4840.

36. Otsuka F, Shimasaki S. A novel function of bone morphogenetic protein-15 in the pituitary: selective synthesis and secretion of FSH by gonadotropes. *Endocrinology* 2002; **143**:4938–4941.
37. Huang HJ, Wu JC, Su P, Zhirnov O, Miller WL. A novel role for bone morphogenetic proteins in the synthesis of follicle-stimulating hormone. *Endocrinology* 2001; **142**:2275–2283.
38. Fredolini C, Bystrom S, Pin E, Edfors F, Tamburro D, Iglesias MJ, Haggmark A, Hong MG, Uhlen M, Nilsson P, Schwenk JM. Immunocapture strategies in translational proteomics. *Expert Rev Proteomics* 2016; **13**:83–98.
39. Anderson RA, Nelson SM, Wallace WH. Measuring anti-Mullerian hormone for the assessment of ovarian reserve: when and for whom is it indicated? *Maturitas* 2012; **71**:28–33.
40. Broer SL, Broekmans FJ, Laven JS, Fauser BC. Anti-Mullerian hormone: ovarian reserve testing and its potential clinical implications. *Hum Reprod Update* 2014; **20**:688–701.
41. Visser JA, Schipper I, Laven JS, Themmen AP. Anti-Mullerian hormone: an ovarian reserve marker in primary ovarian insufficiency. *Nat Rev Endocrinol* 2012; **8**:331–341.
42. Nolan K, Kattamuri C, Luedeke DM, Deng X, Jagpal A, Zhang F, Linhardt RJ, Kenny AP, Zorn AM, Thompson TB. Structure of protein related to Dan and Cerberus: insights into the mechanism of bone morphogenetic protein antagonism. *Structure* 2013; **21**:1417–1429.
43. Brommage R, Liu J, Hansen GM, Kirkpatrick LL, Potter DG, Sands AT, Zambrowicz B, Powell DR, Vogel P. High-throughput screening of mouse gene knockouts identifies established and novel skeletal phenotypes. *Bone Res* 2014; **2**:14034.
44. Khokha MK, Hsu D, Brunet LJ, Dionne MS, Harland RM. Gremlin is the BMP antagonist required for maintenance of Shh and Fgf signals during limb patterning. *Nat Genet* 2003; **34**:303–307.
45. Fenwick MA, Mansour YT, Franks S, Hardy K. Identification and regulation of bone morphogenetic protein antagonists associated with preantral follicle development in the ovary. *Endocrinology* 2011; **152**: 3515–3526.
46. Cimino I, Casoni F, Liu X, Messina A, Parkash J, Jamin SP, Catteau-Jonard S, Collier F, Baroncini M, Dewailly D, Pigny P, Prescott M et al. Novel role for anti-Mullerian hormone in the regulation of GnRH neuron excitability and hormone secretion. *Nat Commun* 2016; **7**:10055.
47. La Marca A, Sighinolfi G, Radi D, Argento C, Baraldi E, Artenisio AC, Stabile G, Volpe A. Anti-Mullerian hormone (AMH) as a predictive marker in assisted reproductive technology (ART). *Hum Reprod Update* 2010; **16**:113–130.
48. Penarrubia J, Fabregues F, Manau D, Creus M, Casals G, Casamitjana R, Carmona F, Vanrell JA, Balasch J. Basal and stimulation day 5 anti-Mullerian hormone serum concentrations as predictors of ovarian response and pregnancy in assisted reproductive technology cycles stimulated with gonadotropin-releasing hormone agonist–gonadotropin treatment. *Hum Reprod* 2005; **20**:915–922.
49. Bristol-Gould SK, Kreeger PK, Selkirk CG, Kilen SM, Cook RW, Kipp JL, Shea LD, Mayo KE, Woodruff TK. Postnatal regulation of germ cells by activin: the establishment of the initial follicle pool. *Dev Biol* 2006; **298**:132–148.
50. Couse JF, Korach KS. Estrogen receptor null mice: what have we learned and where will they lead us? *Endocr Rev* 1999; **20**:358–417.
51. Welt CK, Pagan YL, Smith PC, Rado KB, Hall JE. Control of follicle-stimulating hormone by estradiol and the inhibins: critical role of estradiol at the hypothalamus during the luteal-follicular transition. *J Clin Endocrinol Metab* 2003; **88**:1766–1771.
52. Woodruff T, Krummen L, McCray G, Mather J. *In situ* ligand binding of recombinant human [^{125}I] activin-a and recombinant human [^{125}I] inhibin-a to the adult rat ovary. *Endocrinology* 1993; **133**:2998–3006.
53. Woodruff TK, Besecke LM, Groome N, Draper LB, Schwartz NB, Weiss J. Inhibin A and inhibin B are inversely correlated to follicle-stimulating hormone, yet are discordant during the follicular phase of the rat estrous cycle, and inhibin A is expressed in a sexually dimorphic manner. *Endocrinology* 1996; **137**:5463–5467.
54. Visser JA, de Jong FH, Laven JS, Themmen AP. Anti-Mullerian hormone: a new marker for ovarian function. *Reproduction* 2006; **131**:1–9.
55. Weenen C, Laven JS, Von Bergh AR, Cranfield M, Groome NP, Visser JA, Kramer P, Fauser BC, Themmen AP. Anti-Mullerian hormone expression pattern in the human ovary: potential implications for initial and cyclic follicle recruitment. *Mol Hum Reprod* 2004; **10**:77–83.
56. Wigglesworth K, Lee KB, Emori C, Sugiura K, Eppig JJ. Transcriptomic diversification of developing cumulus and mural granulosa cells in mouse ovarian follicles. *Biol Reprod* 2015; **92**:23.
57. Diaz FJ, Wigglesworth K, Eppig JJ. Oocytes are required for the preantral granulosa cell to cumulus cell transition in mice. *Dev Biol* 2007; **305**:300–311.
58. Convissar S, Armouti M, Fierro MA, Winston NJ, Scoccia H, Zamah AM, Stocco C. Regulation of AMH by oocyte-specific growth factors in human primary cumulus cells. *Reproduction* 2017; **154**:745–753.
59. Pierre A, Estienne A, Racine C, Picard JY, Fanchin R, Lahoz B, Alabart JL, Folch J, Jarrier P, Fabre S, Monniaux D, di Clemente N. The bone morphogenetic protein 15 up-regulates the anti-Mullerian hormone receptor expression in granulosa cells. *J Clin Endocrinol Metab* 2016; **101**:2602–2611.
60. Ogura-Nose S, Yoshino O, Osuga Y, Shi J, Hiroi H, Yano T, Taketani Y. Anti-Mullerian hormone (AMH) is induced by bone morphogenetic protein (BMP) cytokines in human granulosa cells. *Eur J Obstet Gynecol Reprod Biol* 2012; **164**:44–47.
61. Estienne A, Pierre A, di Clemente N, Picard JY, Jarrier P, Mansanet C, Monniaux D, Fabre S. Anti-Mullerian hormone regulation by the bone morphogenetic proteins in the sheep ovary: deciphering a direct regulatory pathway. *Endocrinology* 2015; **156**:301–313.
62. Zhang H, Liu K. Cellular and molecular regulation of the activation of mammalian primordial follicles: somatic cells initiate follicle activation in adulthood. *Hum Reprod Update* 2015; **21**:779–786.
63. Kawamura K, Kawamura N, Hsueh AJ. Activation of dormant follicles: a new treatment for premature ovarian failure? *Curr Opin Obstet Gynecol* 2016; **28**:217–222.
64. Kerr JB, Myers M, Anderson RA. The dynamics of the primordial follicle reserve. *Reproduction* 2013; **146**:R205–R215.
65. Pangas SA. Regulation of the ovarian reserve by members of the transforming growth factor beta family. *Mol Reprod Dev* 2012; **79**: 666–679.
66. Nilsson EE, Skinner MK. Bone morphogenetic protein-4 acts as an ovarian follicle survival factor and promotes primordial follicle development. *Biol Reprod* 2003; **69**:1265–1272.
67. Grgurevic L, Christensen GL, Schulz TJ, Vukicevic S. Bone morphogenetic proteins in inflammation, glucose homeostasis and adipose tissue energy metabolism. *Cytokine Growth Factor Rev* 2016; **27**:105–118.
68. Vukicevic S, Grgurevic L. Bone morphogenetic proteins in inflammation. In: Parnham M (ed.), *Encyclopedia of Inflammatory Disease*. Basel: Springer Verlag; 2015: 1–15.
69. Lakhal B, Laissue P, Braham R, Elghezal H, Saad A, Fellous M, Veitia RA. A novel BMP15 variant, potentially affecting the signal peptide, in a familial case of premature ovarian failure. *Clin Endocrinol (Oxf)* 2009; **71**:752–753.
70. Kumar R, Alwani M, Kosta S, Kaur R, Agarwal S. BMP15 and GDF9 gene mutations in premature ovarian failure. *J Reprod Infertil* 2017; **18**:185–189.
71. Fonseca DJ, Ortega-Recalde O, Esteban-Perez C, Moreno-Ortiz H, Patino LC, Bermudez OM, Ortiz AM, Restrepo CM, Lucena E, Laissue P. BMP15 c.-9C>G promoter sequence variant may contribute to the cause of non-syndromic premature ovarian failure. *Reprod Biomed Online* 2014; **29**:627–633.
72. Renault L, Patino LC, Magnin F, Delemer B, Young J, Laissue P, Binart N, Beau I. BMPR1A and BMPR1B missense mutations cause primary ovarian insufficiency. *J Clin Endocrinol Metab* 2020; **105**.
73. Faure MO, Nicol L, Fabre S, Fontaine J, Mohoric N, McNeilly A, Taragnat C. BMP-4 inhibits follicle-stimulating hormone secretion in ewe pituitary. *J Endocrinol* 2005; **186**:109–121.

74. Bazina M, Vukojevic K, Roje D, Saraga-Babic M. Influence of growth and transcriptional factors, and signaling molecules on early human pituitary development. *J Mol Histol* 2009; **40**:277–286.
75. Sallon C, Faure MO, Fontaine J, Taragnat C. Dynamic regulation of pituitary mRNAs for bone morphogenetic protein (BMP) 4, BMP receptors, and activin/inhibin subunits in the ewe during the estrous cycle and in cultured pituitary cells. *J Endocrinol* 2010; **207**:55–65.
76. Cameron V, Nishimura E, Mathews L, Lewis K, Sawchenko P, Vale W. Hybridization histochemical localization of activin receptor subtypes in rat brain, pituitary, ovary, and testis. *Endocrinology* 1994; **134**:799–808.